# Charged current neutrino and antineutrino induced eta production off the nucleon

A. Fatima, M. Sajjad Athar,[*] and S. K. Singh

*Department of Physics, Aligarh Muslim University, Aligarh-202 002, India*

The charged current (anti)neutrino induced eta production from the nucleons is studied in a model based on the effective Lagrangians to evaluate the contribution from the nonresonant and resonant diagrams. The contribution from the nonresonant background terms has been obtained using a microscopic model based on the SU(3) chiral Lagrangians. The contribution from the resonant diagrams due to the low lying $S_{11}(1535)$, $S_{11}(1650)$, and $P_{11}(1710)$ resonances has been evaluated using an effective phenomenological Lagrangian with its parameters determined from the experimental values of their branching ratios and decay widths to the $N\eta$ channel. The model is first used to reproduce satisfactorily the experimental data from the MAINZ and JLab on the total cross sections for the photo- and electro- production of $\eta$ mesons, which fixes the model parameters in the vector current interaction. The partially conserved axial vector current (PCAC) hypothesis and generalized Goldberger-Treiman relation are used to fix the parameters of the axial vector current interaction. The model is then applied to study the weak production of eta mesons induced by the neutrinos and antineutrinos, and predicts the numerical values for the $Q^2$-distribution, $\eta$-momentum distribution, and the total cross section for the reactions $\nu_\mu + n \rightarrow \mu^- + p + \eta$ and $\bar{\nu}_\mu + p \rightarrow \mu^+ + n + \eta$ in the energy region up to 2 GeV. It is found that the photo, electro, and (anti)neutrino induced production of eta mesons is dominated by the contribution from the $S_{11}(1535)$ resonance. The results discussed in this work are relevant for the present and future accelerator experiments like MicroBooNE, T2K, NOvA, MINERvA, T2-HyperK, and DUNE as well as for the atmospheric neutrino experiments.

## I. INTRODUCTION

Many efforts are being made around the world to understand more about the neutrinos, with the top priorities focused on obtaining the precise information about the mass hierarchy of the neutrino mass states, and the *CP* violating phase delta ($\delta_{CP}$) [1]. Various experiments using the accelerator and the atmospheric neutrinos are being carried out in the few GeV energy region for this purpose. All of these experiments make use of moderate to heavy nuclear targets such as carbon, oxygen, argon, iron, and lead, which necessitate an understanding of the nuclear medium effects that affects the (anti)neutrino-nucleon cross sections when the interaction takes place with the bound nucleons in these nuclei. The study of such nuclear medium effects makes use of a suitable model of the nucleus for describing the nuclear structure along with a good knowledge of the scattering amplitudes for the basic weak

processes of (anti)neutrino scattering from the free nucleons like the neutral current (NC) elastic, charged current (CC) quasielastic, inelastic, and deep inelastic scattering (DIS). While the (anti)neutrino scattering processes of NC elastic, CC quasielastic and DIS from the free nucleons is well studied in the standard model, this is not the case with the inelastic scattering despite the enormous work done on the dominant process of the inelastic single pion production in the region of a few GeV. There are many other inelastic processes, in addition to the single pion production, like the production of kaons, hyperons with (without) accompanying pions, multipions, $\rho$, $\omega$, and $\eta$ mesons, which have not been studied with the same rigor as the single pion production. A study of these processes is important in the region of a few GeV energy where many higher resonances are excited which decay into these particles. Such studies contribute to a better understanding of the various electroweak processes of the excitation of higher resonances in the energy region of shallow inelastic scattering (SIS) leading to the DIS region. The results in the SIS region and their comparison with the results in the DIS region provides an opportunity to understand the phenomenon of quark-hadron duality in electroweak interactions.

In recent years, some work on the kaon and hyperon productions with and without accompanying pions have

been done, but no work has been done on the $\eta$ production except a very early work by Dombey [2] and a recent work by Nakamura et al. [3]. In view of the recent developments in the detector technology, it is possible to experimentally look for the weak production of $\eta$ mesons induced by neutrinos and antineutrinos in present experiments at MicroBooNE, T2K, NOvA, MINERvA, and future experiments at T2-HyperK and DUNE. For example, the MicroBooNE collaboration is currently performing the analysis to study the $\eta$ production cross section [4]. In addition to the additional weak processes of the $\eta$ production, which should be taken into account in modeling the neutrino cross sections being used in various neutrino event generators, the weak production of $\eta$ is an important source probe to search for the strangeness content of the nucleons [5]. Moreover, the weak production of $\eta$ also plays an important role in the background studies in search of the proton decays through the $p \rightarrow \eta e^+$ modes. In view of the topical importance of the weak production of $\eta$, we have studied in this work the CC production of $\eta$ from the free nucleons induced by the (anti)neutrinos through the reactions

$$\nu_\mu + n \rightarrow \mu^- + p + \eta \qquad (1)$$

$$\bar{\nu}_\mu + p \rightarrow \mu^+ + n + \eta \qquad (2)$$

in a model using the effective Lagrangian approach. Separate effective Lagrangians are used to evaluate the contributions of the nonresonant Born terms and the resonant terms. An effective Lagrangian based on SU(3) chiral symmetry is used for the nonresonant Born terms. The basic parameters of the model are $f_m$, the meson decay constants, Cabibbo angle, the proton and neutron magnetic moments, and the axial vector coupling constants for the baryon octet, $D$ and $F$, that are obtained from the analysis of the semileptonic decays of neutron and hyperons. We consider low lying $I = \frac{1}{2}$ resonances such as $S_{11}(1535)$, $S_{11}(1650)$, and $P_{11}(1710)$. The vector form factors of the $N - S_{11}$ and $N - P_{11}$ transitions have been obtained from the helicity amplitudes extracted in the analysis of pion photo- and electro- production data using the MAID analysis in the unitary isobar model [6]. The present model has been earlier used to study the associated particle production using real photons off the proton target [7], weak interaction induced single pion production [8], kaon production [9–11], two pion production [12], etc. For a detailed description, please see Ref. [13].

First, we have applied this model to obtain the results of the cross sections for photo- and electro-induced eta production off the nucleon target. The production of $\eta$ particle in electromagnetic reactions induced by photons and electrons is well studied experimentally, with the availability of high-duty cycle electron accelerators, such as the MIT-Bates, ELSA at Bonn, MAMI at Mainz,

NIKHEF at Watergraafsmeer, and CEBAF at JLab [14–24]. Recently, results have been reported from MAMI-C [18] using Crystal Ball and TAPS multi photon spectrometer in the energy range of 707 MeV to 1.4 GeV for the differential as well as the total scattering cross sections. In theoretical studies of the $\eta$ production in the electromagnetic reactions induced by photons and electrons [25–43], the contribution of the vector current is fairly known. We find that the theoretical results obtained in this model explain well the photoproduction total cross section data from CLAS 2006 [44] for $\gamma + p \rightarrow \Lambda + K$, and the photoproduction data from MAMI Crystal Ball [18,19] for $\gamma + p \rightarrow p + \eta$ and $\gamma + n \rightarrow n + \eta$, and the electroproduction data from CLAS 2001 [16] for $e + p \rightarrow e + p + \eta$. These results have been used to fix the electromagnetic vector couplings and the $Q^2$ dependence of the vector $N - R$ transition form factors. This information is then used to obtain the isovector vector form factors for $N - R$ transitions. The axial vector coupling is fixed using the experimental $S_{11} \rightarrow N\pi$ and $P_{11} \rightarrow N\pi$ partial decay widths. Assuming the pion-pole dominance together with the PCAC hypothesis, the pseudoscalar form factor is obtained in terms of the axial vector form factor. For the $Q^2$ dependence of the axial vector form factor, we have used a dipole form with the value of axial dipole mass taken to be $M_A = 1$ GeV.

The plan of the paper is following. In Secs. II A and II B, we present the formalism for photon and electron induced eta production, respectively. In Sec. II C, the formalism for the charged current $\nu_l(\bar{\nu}_l)$ induced eta production has been presented. The results and discussions are presented in Sec. III, and Sec. IV concludes our findings.

## II. FORMALISM

The eta meson is an isoscalar pseudoscalar particle ($I = 0, J^P = 0^-$), a member of the ground state SU(3) meson nonet with mass 547.86 MeV, a life time of about $5 \times 10^{-19}$ sec and decays mainly to $3\pi\,(\sim56\%)$, $2\gamma\,(\sim39\%)$, and $\pi^+\pi^-\gamma\,(\sim4.5\%)$ modes. The $\eta$ mesons are produced at $E_{\nu_l(\bar{\nu}_l)} \geq 0.71(0.88)$ GeV for $\nu_e(\nu_\mu)$ induced CC reactions. In the following sections, we have first applied our model to study the electromagnetic production of eta mesons induced by real and virtual photons, followed by the weak production of eta induced by (anti)neutrinos from the free nucleon target.

### A. $\eta$ production induced by photons

The differential cross section for the photoproduction of $\eta$ meson off the free nucleon, i.e.,

$$\gamma(q) + N(p) \rightarrow N(p') + \eta(p_\eta), \qquad (3)$$

is written as

$$d\sigma = \frac{1}{4(q \cdot p)}(2\pi)^4 \delta^4(q + p - p_\eta - p')\frac{d\vec{p}_\eta}{(2\pi)^3(2E_\eta)}$$

$$\times \frac{d\vec{p}'}{(2\pi)^3(2E')}\overline{\sum_r}\sum |\mathcal{M}^r|^2, \tag{4}$$

where $N = p$ or $n$, the quantities in the parentheses of Eq. (3) represent the four momenta of the corresponding particles, $E_\eta$ and $E'$, respectively, are the energies of the outgoing eta and nucleon. $\overline{\sum}\sum |\mathcal{M}^r|^2$ is the square of the transition matrix element $\mathcal{M}^r$, for the photon polarization state $r$, averaged and summed over the initial and final spin states.

Using Eq. (4), the differential cross section $\frac{d\sigma}{d\Omega}$ in the c.m. frame (Fig. 1) is written as

$$\left.\frac{d\sigma}{d\Omega}\right|_{\text{c.m.}} = \frac{1}{64\pi^2 s}\frac{|\vec{p}'|}{|\vec{p}|}\overline{\sum_r}\sum_{\text{spin}} |\mathcal{M}^r|^2, \tag{5}$$

where the c.m. energy $\sqrt{s}$ is obtained as

$$s = W^2 = (q + p)^2 = M^2 + 2ME_\gamma, \tag{6}$$

with $E_\gamma$ being the energy of the incoming photon in the laboratory frame.

In the above expression, the transition matrix element $\mathcal{M}^r$ for the reaction (3) is written in terms of the real photon polarization vector $\epsilon_\mu^r$, i.e.

$$\mathcal{M}^r = e\epsilon_\mu^r(q)J^\mu, \tag{7}$$

where $e = \sqrt{4\pi\alpha}$ with $\alpha$ being the fine-structure constant, $J^\mu = \langle N(p')\eta(p_\eta)|J_{\text{EM}}^\mu|N(p)\rangle$ is the matrix element of the electromagnetic current ($J_{\text{EM}}^\mu$) taken between the hadronic states $|N\rangle$ and $|N\eta\rangle$, and $\epsilon_\mu^r(q)$ satisfy the condition
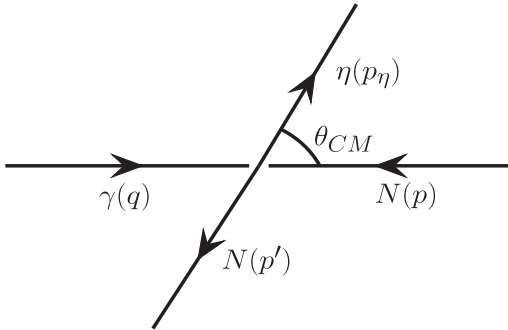


FIG. 1. Diagrammatic representation of the process $\gamma(q) + N(p) \rightarrow \eta(p_\eta) + N(p')$ in the center of mass (c.m.) frame. The quantities in the parentheses represent the four momenta of the corresponding particles. $\theta^{\text{c.m.}}$ is the angle between photon and eta in the c.m. frame.

$$\sum_{r=\pm1} \epsilon_\mu^{*(r)}\epsilon_\nu^{(r)} \rightarrow -g_{\mu\nu}. \tag{8}$$

The hadronic tensor $\mathcal{J}^{\mu\nu}$ is defined in terms of the hadronic current $J^\mu$ as

$$\mathcal{J}^{\mu\nu} = \overline{\sum}\sum_{\text{spins}} J^{\mu\dagger}J^\nu = \text{Tr}[(\not{p} + M)\tilde{J}^\mu(\not{p}' + M')J^\nu],$$

$$\tilde{J}^\mu = \gamma_0(J^\mu)^\dagger\gamma_0, \tag{9}$$

where $M$ and $M'$ are the masses of the incoming and outgoing nucleons, respectively. The hadronic matrix element receives contributions from the nonresonant background terms and the terms corresponding to the resonance excitations, which diagrammatically are shown in Fig. 2. The total current $J^\mu$ is therefore written as:

$$J^\mu = J_{\text{NR}}^\mu + J_R^\mu e^{i\Phi} \tag{10}$$

where $\Phi$ is the relative phase with which the hadronic current corresponding to the nonresonant ($J_{\text{NR}}^\mu$) and the resonance ($J_R^\mu$) terms are added. In the case of pion production, the value of $\Phi$ is generally taken as zero [45–47] and the currents are added coherently. We have followed the same prescription, in the case of $\eta$ production, and added the currents corresponding to the nonresonant and resonance terms coherently. The hadronic currents for the various nonresonant terms shown in Fig. 2 are obtained using the nonlinear sigma model which in the following has been discussed very briefly. The explicit expressions for the hadronic currents are given in Sec. II A 2 for the nonresonant and the resonance terms.

Using Eqs. (8) and (9), the transition matrix element squared is obtained as

$$\overline{\sum_r}\sum_{\text{spin}} |\mathcal{M}^r|^2 = -\frac{e^2}{4}g_{\mu\nu}\mathcal{J}^{\mu\nu}, \tag{11}$$

used for the cross sections defined in Eq. (5).

### 1. Nonlinear sigma model

The lowest-order $SU(3)$ chiral Lagrangian in the nonlinear sigma model describing the pseudoscalar mesons in the presence of an external current, is given by [48,49]:

$$\mathcal{L}_M = \frac{f_m}{4}\text{Tr}[D_\mu U(D^\mu U)^\dagger]. \tag{12}$$

The covariant derivatives $D^\mu U$ and $D^\mu U^\dagger$ appearing in Eq. (12) are expressed in terms of the partial derivatives as

$$D^\mu U \equiv \partial^\mu U - ir^\mu U + iUl^\mu,$$

$$D^\mu U^\dagger \equiv \partial^\mu U^\dagger + iU^\dagger r^\mu - il^\mu U^\dagger, \tag{13}$$
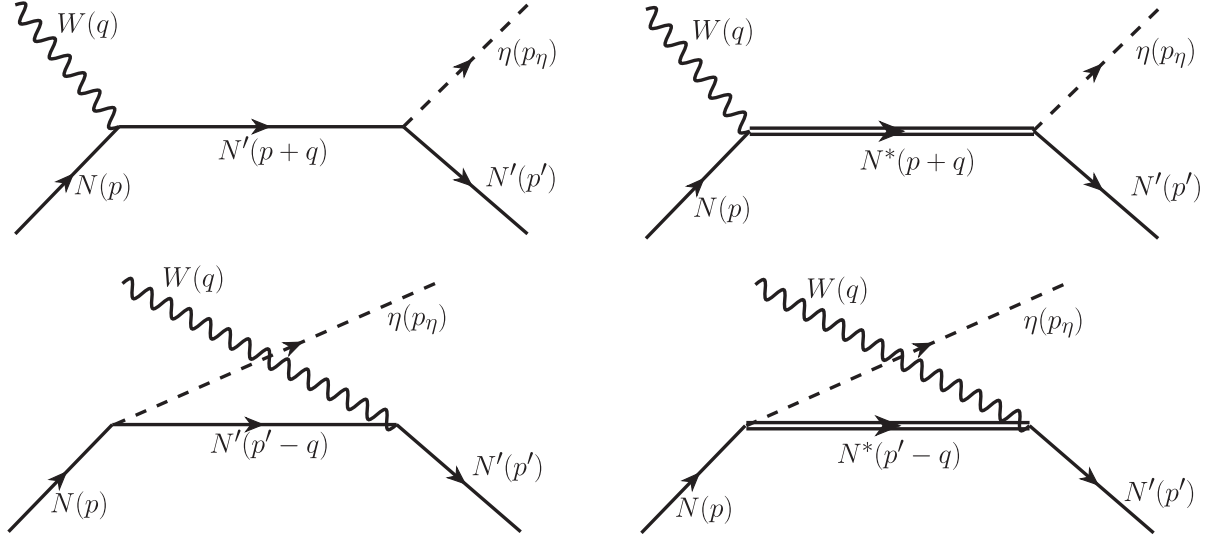
FIG. 2.   Feynman diagrams corresponding to the nonresonant Born terms (left panel) and resonance excitations (right panel) for the process $\gamma(q) + N(p) \to \eta(p_\eta) + N(p')$. Diagrams shown in the top panel are the nucleon pole diagrams, while the one shown in the bottom panel corresponds to the cross nucleon pole diagrams. In the case of electromagnetic interactions, $W = \gamma, \gamma^*$ and $N' = N = p, n$, while in the case of CC induced weak interactions, $W = W^\pm$ and $N'$ and $N$ corresponds to the different nucleons depending upon the charge conservation. The quantities in the parentheses represent the four momenta of the corresponding particles.

where $U$ is the $SU(3)$ unitary matrix given as

$$U(x) = \exp\left(i\frac{\Phi(x)}{f_m}\right), \qquad (14)$$

where $f_m$ is the meson decay constant, $\Phi(x)$ corresponds to the $3 \times 3$ pseudoscalar meson matrix. $r_\mu$ and $l_\mu$, respectively, represent the right and left handed currents, defined in terms of the vector ($v_\mu$) and axial-vector ($a_\mu$) fields as

$$l_\mu = \frac{1}{2}(v_\mu - a_\mu), \qquad r_\mu = \frac{1}{2}(v_\mu + a_\mu). \qquad (15)$$

The vector and axial-vector fields are different for the interaction of the different gauge boson fields with the meson fields.

In the case of electromagnetic gauge fields, the left and right handed currents are identical and are expressed as

$$l_\mu = r_\mu = -e\hat{Q}A_\mu, \qquad (16)$$

where $e$ is the strength of the electromagnetic interaction, $A_\mu$ represents the photon field and

$$\hat{Q} = \begin{pmatrix} 2/3 & 0 & 0 \\ 0 & -1/3 & 0 \\ 0 & 0 & -1/3 \end{pmatrix}$$

represents the charge of the $u$, $d$, and $s$ quarks. In the case of weak CC induced processes, the left and right handed currents are expressed as

$$l_\mu = -\frac{g}{2}(W_\mu^+ T_+ + W_\mu^- T_-), \qquad r_\mu = 0, \qquad (17)$$

where $g = \frac{e}{\sin\theta_W}$, $\theta_W$ is the Weinberg angle, $W_\mu^\pm$ represents the W-boson field and $T_\pm$ is defined as

$$T_+ = \begin{pmatrix} 0 & V_{ud} & V_{us} \\ 0 & 0 & 0 \\ 0 & 0 & 0 \end{pmatrix}, \quad \text{and} \quad T_- = \begin{pmatrix} 0 & 0 & 0 \\ V_{ud} & 0 & 0 \\ V_{us} & 0 & 0 \end{pmatrix}, \qquad (18)$$

with $V_{ud} = \cos\theta_C$ and $V_{us} = \sin\theta_C$ being the elements of the Cabibbo-Kobayashi-Maskawa matrix and $\theta_C$ being the Cabibbo angle.

The lowest-order chiral Lagrangian for the baryon octet in the presence of an external current, may be written in terms of the $SU(3)$ matrix of the baryons $B$ as [48,49],

$$\mathcal{L}_{MB} = \text{Tr}[\bar{B}(i\slashed{D} - M)B] - \frac{D}{2}\text{Tr}(\bar{B}\gamma^\mu\gamma_5\{u_\mu, B\}) - \frac{F}{2}\text{Tr}(\bar{B}\gamma^\mu\gamma_5[u_\mu, B]), \qquad (19)$$

where $M$ denotes the mass of the baryon octet, $D = 0.804$ and $F = 0.463$ are the symmetric and antisymmetric axial-vector coupling constants for the baryon octet, and the Lorentz vector $u^\mu$ is given by [49]:

$$u^\mu = i[u^\dagger(\partial^\mu - ir^\mu)u - u(\partial^\mu - il^\mu)u^\dagger]. \qquad (20)$$

In the case of meson-baryon interactions, the unitary matrix for the pseudoscalar field is expressed as

$$u = \sqrt{U} \equiv \exp\left(i\frac{\Phi(x)}{2f_m}\right), \qquad (21)$$

and the covariant derivative $D_\mu$ on the baryon fields $B$ is given by

$$D_\mu B = \partial_\mu B + [\Gamma_\mu, B], \quad \text{with}$$
$$\Gamma^\mu = \frac{1}{2}[u^\dagger(\partial^\mu - ir^\mu)u + u(\partial^\mu - il^\mu)u^\dagger], \qquad (22)$$

which is known as the chiral connection.

### 2. Currents for the nonresonant Born terms and resonance excitations

Expanding the Lagrangians given in Eqs. (12) and (19) for the lowest lying baryons and mesons, one obtains the Lagrangians for any desired vertex involving the interactions of mesons and baryons among themselves or with the external fields. Using these Lagrangians, the expressions of the hadronic currents for $s$-, $u$-channels of the $\eta$ photoproduction processes, corresponding to the Feynman diagrams shown in Fig. 2 (left panel), are obtained as [13]:

$$J^\mu|_{sN} = -A_s F_s(s)\bar{u}(p')\slashed{p}_\eta\gamma_5\frac{\slashed{p}+\slashed{q}+M}{s-M^2}$$
$$\times \left(\gamma^\mu e_N + i\frac{\kappa_N}{2M}\sigma^{\mu\nu}q_\nu\right)u(p), \qquad (23)$$

$$J^\mu|_{uN} = -A_u F_u(u)\bar{u}(p')\left(\gamma^\mu e_N + i\frac{\kappa_N}{2M}\sigma^{\mu\nu}q_\nu\right)$$
$$\times \frac{\slashed{p}'-\slashed{q}+M}{u-M^2}\slashed{p}_\eta\gamma_5 u(p), \qquad (24)$$

where $N$ stands for a proton or a neutron in the initial and final states, $s$ is defined in Eq. (6) and $u = (p'-q)^2$, $A_i$'s; $i = s$, $u$ are the coupling strengths of $s$, and $u$ channels, respectively, and are obtained as [13]

$$A_s = A_u = \left(\frac{D - 3F}{2\sqrt{3}f_\eta}\right). \qquad (25)$$

$D$ and $F$ are the axial-vector couplings of the baryon octet and $f_\eta = 105$ MeV [50] is the $\eta$ decay constant. The value of $\kappa$ for proton, and neutron are $\kappa_p = 1.7928$, and $\kappa_n = -1.913$ in units of $\mu_N$ [51].

In order to take into account the hadronic structure of the nucleons, the form factors $F_s(s)$, and $F_u(u)$, are introduced at the strong vertex. Various parametrizations of these form factors are available in the literature [52]. We use the most

general form of the hadronic form factor which is taken to be of the dipole form [7]:

$$F_x(x) = \frac{\Lambda_B^4}{\Lambda_B^4 + (x - M_x^2)^2}, \qquad x = s, u, \qquad (26)$$

where $\Lambda_B$ is the cutoff parameter taken to be the same for the s- and u-channel nonresonant Born terms. $x$ represents the Mandelstam variables $s$, $u$, and $M_x = M$ corresponds to the mass of the exchanged nucleons in the $s$ and $u$ channels. The value of $\Lambda_B$ is fitted to the experimental data for both the proton and neutron targets simultaneously and the best fitted value is $\Lambda_B = 0.78$ GeV for s- and u-channel diagrams. One of the most important property of the electromagnetic current is the gauge invariance which ensures the current conservation and is implemented in the case of $\eta$ production.

In the present work, we have taken into account only the low lying resonances, which have mass $M_R < 1.8$ GeV and have a significant branching ratio to the $N\eta$ mode reported in PDG [51]. Specifically, we have considered three spin $\frac{1}{2}$ resonances viz. $S_{11}(1535)$, $S_{11}(1650)$, and $P_{11}(1710)$. The general properties of these resonances like mass, decay width, spin, etc. are given in Table I, where we see that $S_{11}(1535)$ resonance dominates the coupling to the $N\eta$ channel.

The hadronic vector transition current for the spin $\frac{1}{2}$ resonance state is given by [53]

$$j^\mu_{\frac{1}{2}} = \bar{u}(p')\Gamma^\mu_{\frac{1}{2}}u(p), \qquad (27)$$

where $u(p)$ and $\bar{u}(p')$ are, respectively, the Dirac spinor and the adjoint Dirac spinor for spin $\frac{1}{2}$ particles and $\Gamma^\mu_{\frac{1}{2}}$ is the vertex function. For a positive parity state, $\Gamma^\mu_{\frac{1}{2}^+}$ is given by

$$\Gamma^\mu_{\frac{1}{2}^+} = V^\mu_{\frac{1}{2}}, \qquad (28)$$

and for a negative parity resonance, $\Gamma^\mu_{\frac{1}{2}^-}$ is given by

$$\Gamma^\mu_{\frac{1}{2}^-} = V^\mu_{\frac{1}{2}}\gamma_5, \qquad (29)$$

where $V^\mu_{\frac{1}{2}}$ represents the vector current parametrized in terms of $F_2^{R^+,R^0}$, as

$$V^\mu_{\frac{1}{2}} = \left[\frac{F_2^{R^+,R^0}}{2M}i\sigma^{\mu\alpha}q_\alpha\right]. \qquad (30)$$

The coupling $F_2^{R^+,R^0}$ is derived from the helicity amplitudes extracted from the real photon scattering experiments.

TABLE I. Properties of the spin $\frac{1}{2}$ resonances available in the PDG [51], with Breit-Wigner mass $M_R$, the total decay width $\Gamma_R$, isospin $I$, spin $J$, parity $P$, the branching ratio full range available from PDG (used in the present calculations) into different meson-baryon like $N\pi$, $N\eta$, $K\Lambda$, and $N\pi\pi$, and the strong coupling constant $g_{RN\pi}$ and $g_{RN\eta}$.

| Resonance → Parameters ↓ | | $S_{11}(1535)$ | $S_{11}(1650)$ | $P_{11}(1710)$ |
|---|---|---|---|---|
| $M_R$ (GeV) | | $1.510 \pm 0.01$ | $1.655 \pm 0.015$ | $1.700 \pm 0.02$ |
| $\Gamma_R$ (GeV) | | $0.130 \pm 0.02$ | $0.135 \pm 0.035$ | $0.120 \pm 0.04$ |
| $I(J^P)$ | | $\frac{1}{2}(\frac{1}{2}^-)$ | $\frac{1}{2}(\frac{1}{2}^-)$ | $\frac{1}{2}(\frac{1}{2}^+)$ |
| Branching ratio (in %) | $N\pi$ | 32–52 (43) | 50–70 (60) | 5–20 (16) |
| | $N\eta$ | 30–55 (40) | 15–35 (25) | 10–50 (20) |
| | $K\Lambda$ | – | 5–15 (10) | 5–25 (15) |
| | $N\pi\pi$ | 4–11 (17) | 20–58 (5) | 14–48 (49) |
| $|g_{RN\pi}|$ | | 0.1019 | 0.0915 | 0.0418 |
| $|g_{RN\eta}|$ | | 0.3696 | 0.1481 | 0.1567 |

The explicit relation between the coupling $F_2^{R^+,R^0}$ and the helicity amplitude $A_{\frac{1}{2}}^p$ is given by [7]:

$$A_{\frac{1}{2}}^{p,n} = \sqrt{\frac{2\pi\alpha}{M}\frac{(M_R \mp M)^2}{M_R^2 - M^2}}\left[\frac{M_R \pm M}{2M}F_2^{R^+,R^0}\right], \quad (31)$$

where the upper (lower) sign stands for the positive (negative) parity resonance. $R^+$ and $R^0$ correspond, respectively, to the charged and neutral states of the isospin $\frac{1}{2}$ resonances. $M_R$ is the mass of corresponding resonance. The value of the helicity amplitude $A_{\frac{1}{2}}^{p,n}$ for the $S_{11}(1650)$ resonance is taken from MAID [54], while for the other spin $\frac{1}{2}$ nucleon resonances, these values are taken from PDG [51] and are quoted in Table II.

The most general form of the hadronic currents for the $s-$ and $u-$channel processes where a resonance state $R_{\frac{1}{2}}$ is produced and decays to a $\eta$ and a nucleon in the final state, are written as

TABLE II. Parametrization of the transition form factors for $S_{11}(1535)$, $S_{11}(1650)$, $P_{11}(1710)$ resonances on the proton and neutron targets. $\mathcal{A}_\alpha(0)$ is given in units of $10^{-3}$ GeV$^{-2}$ and the coefficients $a_1$ and $b_1$ in units of GeV$^{-2}$.

| | | Proton target | | | Neutron target | | |
|---|---|---|---|---|---|---|---|
| Resonance | Helicity amplitude | $\mathcal{A}_\alpha(0)$ | $a_1$ | $b_1$ | $\mathcal{A}_\alpha(0)$ | $a_1$ | $b_1$ |
| $S_{11}(1535)$ | $A_{\frac{1}{2}}$ | 95.0 | 0.5 | 0.51 | −78.0 | 1.75 | 1.75 |
| | $S_{\frac{1}{2}}$ | −2.0 | 23.9 | 0.81 | 32.5 | 0.4 | 1.0 |
| $S_{11}(1650)$ | $A_{\frac{1}{2}}$ | 33.3 | 1.45 | 0.62 | 26.0 | 0.1 | 2.5 |
| | $S_{\frac{1}{2}}$ | −3.5 | 2.88 | 0.76 | 3.8 | 0.4 | 0.71 |
| $P_{11}(1710)$ | $A_{\frac{1}{2}}$ | 50.0 | 1.4 | 0.95 | −45.0 | −0.02 | 0.95 |
| | $S_{\frac{1}{2}}$ | 27.4 | 0.18 | 0.88 | −31.5 | 0.35 | 0.85 |

$$j^\mu|_s = \frac{g_{RN\eta}}{f_\eta}\bar{u}(p')\slashed{p}_\eta\Gamma_s\left(\frac{\slashed{p} + \slashed{q} + M_R}{s - M_R^2 + iM_R\Gamma_R}\right)\Gamma^\mu_{\frac{1}{2}\pm}u(p),$$

$$j^\mu|_u = \frac{g_{RN\eta}}{f_\eta}\bar{u}(p')\Gamma^\mu_{\frac{1}{2}\pm}\left(\frac{\slashed{p}' - \slashed{q} + M_R}{u - M_R^2 + iM_R\Gamma_R}\right)\slashed{p}_\eta\Gamma_s u(p),$$

$$(32)$$

where $\Gamma_R$ is the decay width of the resonance, $\Gamma_s = 1(\gamma_5)$ stands for the positive (negative) parity resonances. $\Gamma_{\frac{1}{2}^+}$ and $\Gamma_{\frac{1}{2}^-}$ are, respectively, the vertex functions for the positive and negative parity resonances, defined in Eqs. (65) and (66), respectively. $g_{RN\eta}$ is the coupling strength for the process $R \to N\eta$, given in Table I.

We determine the $RN\eta$ coupling using the value of branching ratio and decay width of these resonances from PDG [51] and use the expression for the decay rate which is obtained by writing the most general form of $RN\eta$ Lagrangian [55]:

$$\mathcal{L}_{RN\eta} = \frac{g_{RN\eta}}{f_\eta}\bar{\Psi}_R\Gamma^\mu_s\partial_\mu\eta^i\tau_i\Psi, \quad (33)$$

where $g_{RN\eta}$ is the $RN\eta$ coupling strength. $\Psi$ is the nucleon field and $\Psi_R$ is the resonance field. $\eta^i$ is the eta field and $\tau$ is the isospin factor for the isospin $\frac{1}{2}$ states. The interaction vertex $\Gamma^\mu_s = \gamma^\mu\gamma^5$ $(\gamma^\mu)$ stands for positive (negative) parity resonance states.

Using the above Lagrangian, one obtains the expression for the decay width in the resonance rest frame as [13]:

$$\Gamma_{R\to N\eta} = \frac{\mathcal{C}}{4\pi}\left(\frac{g_{RN\eta}}{f_\eta}\right)^2(M_R \pm M)^2\frac{E_N \mp M}{M_R}|\vec{p}_\eta^{\,cm}|, \quad (34)$$

where the upper (lower) sign represents the positive (negative) parity resonance. The parameter $\mathcal{C}$ depends upon the charged state of $R$, $N\eta$ and is obtained from the isospin

analysis and found out to be 1. $|\vec{p}_\eta^{cm}|$ is the outgoing eta momentum measured from the resonance rest frame and is given by,

$$|\vec{p}_\eta^{\text{cm}}| = \frac{\sqrt{(W^2 - M_\eta^2 - M^2)^2 - 4M_\eta^2 M^2}}{2M_R} \qquad (35)$$

and $E_N$, the outgoing nucleon energy is

$$E_N = \frac{W^2 + M^2 - M_\eta^2}{2M_R}, \qquad (36)$$

where $W$ is the total center of mass energy carried by the resonance.

In analogy with the nonresonant terms, we have considered the following form factors at the strong vertex, in order to take into account the hadronic structure:

$$F_x^*(x) = \frac{\Lambda_R^4}{\Lambda_R^4 + (x - M_x^2)^2}, \qquad (37)$$

where $\Lambda_R$ is the cutoff parameter whose value is fitted to the experimental data, $x$ represents the Mandelstam variables $s$, $u$, and $M_x = M_R$ corresponding to the mass of the nucleon resonances exchanged in the $s$, and $u$ channels. In general, $\Lambda_R$ would be different from $\Lambda_B$, however, in the case of $\eta$ production by photons, it happens that the same value of $\Lambda_R$

as that of $\Lambda_B$, i.e., $\Lambda_R = \Lambda_B = 0.78$ GeV gives the best fit to the experimental data. The same values of $\Lambda_R$ and $\Lambda_B$ help us to minimize the number of free parameters used to fit the experimental data.

In Fig. 3, we have presented the results for the total scattering cross section $\sigma$ as a function of $W$ for $\gamma + p \to p + \eta$ and $\gamma + n \to n + \eta$ processes in the region of $W$ from $\eta$ production threshold to $K\Lambda$ production threshold. We have compared our theoretical results with the experimental data obtained by McNicoll *et al.* [18] for the MAMI crystal ball collaboration on the proton target and the quasifree neutron data from Werthmuller *et al.* [19] for the MAMI A2 collaboration. It may be observed from the figure that in the case of $\eta$ production from the proton and neutron targets, our results, with a very few free parameters, are in a very good agreement with the available experimental data. To show the dominance of $S_{11}(1535)$ resonance in the first peak region, we have also presented the results obtained by switching off $S_{11}(1535)$ resonance. It may be noticed that the first peak in the case of $p\eta$ as well as $n\eta$ channels is dominated only by $S_{11}(1535)$ resonance.

### B. Electroproduction of eta meson

The electron induced $\eta$ production off the nucleon target is given by the reaction

$$e^-(k) + N(p) \to e^-(k') + N(p') + \eta(p_\eta), \qquad (38)$$

where the four-momentum for each particle is indicated in the parentheses. The four-momentum of the virtual photon exchanged in electroproduction is given by $q = k - k'$.

The differential cross section for the electroproduction process can be written as

$$d\sigma = \frac{1}{4ME_e(2\pi)^5} \frac{d\vec{k}'}{(2E_l)} \frac{d\vec{p}'}{(2E_N)} \frac{d\vec{p}_\eta}{(2E_\eta)} \delta^4(k + p - k' - p' - p_\eta)$$

$$\times \overline{\sum} \sum |\mathcal{M}|^2, \qquad (39)$$

where $k(k')$ is the four momentum of the incoming (outgoing) electron with energy $E_e(E_l)$; $p$ is the four momentum of the incoming nucleon which is at rest, $E_N$ and $p'$ are respectively the energy and four momentum of the outgoing nucleon, and the four momentum of $\eta$ is $p_\eta$ with energy $E_\eta$, and $M$ is the nucleon mass. The different kinematical variables used in the numerical calculations of the scattering cross section are depicted in Fig. 4, where the scattering plane is in the laboratory frame while the reaction plane is in the center of mass (c.m.) frame. $\overline{\sum} \sum |\mathcal{M}|^2$ is the square of the transition amplitude averaged (summed) over the spins of the initial (final) states and the transition matrix element is written in terms of the leptonic and the hadronic currents as
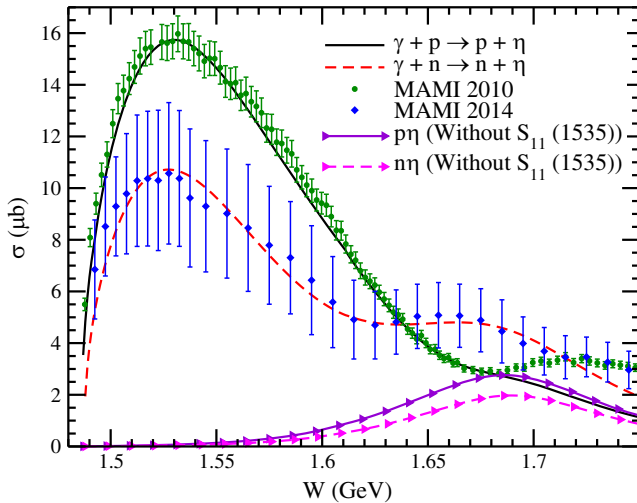


FIG. 3. Total cross section $\sigma$ vs. $W$ for $\gamma p \to \eta p$ (solid line) and $\gamma n \to \eta n$ (dashed line) processes using the full model. The results obtained when the contribution of $S_{11}(1535)$ resonance is switched off are shown here by a solid line with triangles (dashed line with triangles) for $p\eta(n\eta)$ production channels. The experimental points for the proton target (solid circle) are obtained from MAMI crystal ball collaboration [18], and for the neutron target (solid diamond) we have used the quasifree neutron data from MAMI A2 collaboration [19].
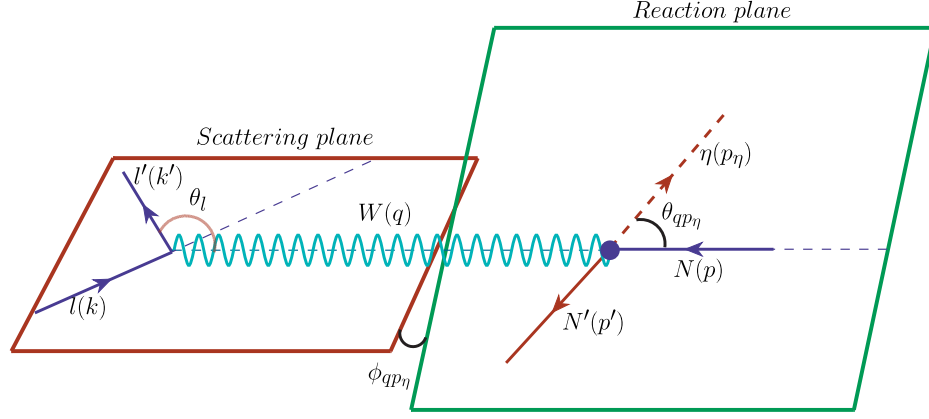
FIG. 4.  Electron (electromagnetic)/(anti)neutrino (weak) scattering and reaction planes, depicting the hadronic plane in c.m. frame and scattering plane in the laboratory frame. The kinematical variables used in the calculation of the scattering cross sections are defined in the figure.

$$\mathcal{M} = \frac{e^2}{q^2} l_\mu j^\mu, \tag{40}$$

where $l_\mu$ and $j^\mu$, respectively, are the leptonic and hadronic currents. The leptonic current is given as

$$l_\mu = \bar{u}(k')\gamma_\mu u(k), \tag{41}$$

and $j^\mu$ is the sum of the hadronic currents corresponding to the Born terms and resonance excitations, which will be discussed later in Sec. II B 1.

Integrating over the three momentum of the outgoing nucleon, the expression for the differential scattering cross section given in Eq. (39) in the hadronic c.m. frame becomes

$$\frac{d^5\sigma}{dE_l d\Omega_l d\Omega_{qp_\eta}} = \frac{1}{32(2\pi)^5} \frac{|\vec{k}'||\vec{p}_\eta|}{E_e MW} \overline{\sum}\sum |\mathcal{M}|^2. \tag{42}$$

The fivefold differential cross section for the electroproduction can also be expressed as [56–58]:

$$\frac{d\sigma}{d\Omega_l dE_l d\Omega_{qp_\eta}} = \Gamma \frac{d\sigma_{\rm v}}{d\Omega_{qp_\eta}}, \tag{43}$$

with the flux of the virtual photon field given by

$$\Gamma = \frac{\alpha}{2\pi^2} \frac{E_l}{E_e} \frac{K}{Q^2} \frac{1}{1-\varepsilon}. \tag{44}$$

In the above equation, $K = (W^2 - M^2)/2M$ denotes the "photon equivalent energy," the laboratory energy necessary for a real photon to excite a hadronic system with c.m. energy $W$. The transverse polarization parameter of the virtual photon

$$\varepsilon = \left(1 + 2\frac{|\vec{q}|^2}{Q^2} \tan^2 \frac{\theta_l}{2}\right)^{-1}, \tag{45}$$

where $Q^2 = -q^2 = -(k-k')^2$.

It is useful to express the angular distribution of the eta mesons in the c.m. frame of the final hadronic states, particularly for the use of multipole decompositions. Therefore, the virtual photon cross section $d\sigma_{\rm v}/d\Omega$ should be evaluated in the c.m. frame, while the fivefold differential cross section in Eq. (43) is interpreted with the flux factor in the lab frame. By choosing the energies of the initial and final electrons and the scattering angle $\theta_l$ (see Fig. 4), we can fix the momentum transfer $Q^2$ and the polarization parameter $\varepsilon$ of the virtual photon.

### 1. Currents for the nonresonant Born terms and resonance excitations

Currents corresponding to the nucleon Born terms for the electroproduction of eta mesons, depicted in Fig. 2, are obtained using the nonlinear sigma model discussed in Sec. II A 1 and are written as:

$$J^\mu_{N(s)} = \frac{D-3F}{2\sqrt{3}f_\eta} \bar{u}_N(p') \slashed{p}_\eta \gamma^5 \frac{\slashed{p} + \slashed{q} + M}{(p+q)^2 - M^2} \mathcal{O}^\mu_N u_N(p)$$

$$J^\mu_{N(u)} = \frac{D-3F}{2\sqrt{3}f_\eta} \bar{u}_N(p') \mathcal{O}^\mu_N \frac{\slashed{p} - \slashed{p}_\eta + M}{(p-p_\eta)^2 - M^2} \slashed{p}_\eta \gamma^5 u_N(p), \tag{46}$$

where the $\gamma NN$ vertex operator $\mathcal{O}^\mu_N$ is expressed in terms of the $Q^2$ dependent nucleon form factors as,

$$\mathcal{O}^\mu_N = F_1^N(Q^2)\gamma^\mu + F_2^N(Q^2) i\sigma^{\mu\nu} \frac{q_\nu}{2M}. \tag{47}$$

The Dirac and Pauli form factors of the nucleon viz. $F_1^{p,n}(Q^2)$ and $F_2^{p,n}(Q^2)$, respectively, may be expressed

in terms of the Sach's electric $[G_E^{p,n}(Q^2)]$ and magnetic $[G_M^{p,n}(Q^2)]$ form factors of the nucleons as,

$$
F_1^{p,n}(Q^2) = \left(1 + \frac{Q^2}{4M^2}\right)^{-1}\left[G_E^{p,n}(Q^2) + \frac{Q^2}{4M^2}G_M^{p,n}(Q^2)\right]
$$
$$
F_2^{p,n}(Q^2) = \left(1 + \frac{Q^2}{4M^2}\right)^{-1}[G_M^{p,n}(Q^2) - G_E^{p,n}(Q^2)]. \quad (48)
$$

There are various parametrization for $G_{E,M}^{p,n}(Q^2)$ those are available in the literature. For the present work we have taken the parametrization of these form factors from Bradford *et al.* [59], also known as BBBA05 parametrization.

Now we discuss the hadronic current corresponding to the resonance excitations and their subsequent decay to $N\eta$ channel. The general expression of the hadronic current for the resonance excitation in the s- and u-channels, corresponding to the Feynman diagrams shown in Fig. 2 (right panel), are written, as,

$$
j^\mu|_s = \frac{g_{RN\eta}}{f_\eta}\bar{u}(p')\slashed{p}_\eta\Gamma_s\left(\frac{\slashed{p} + \slashed{q} + M_R}{s - M_R^2 + iM_R\Gamma_R}\right)\Gamma_{\frac{1}{2}\pm}^\mu u(p),
$$
$$
j^\mu|_u = \frac{g_{RN\eta}}{f_\eta}\bar{u}(p')\Gamma_{\frac{1}{2}\pm}^\mu\left(\frac{\slashed{p}' - \slashed{q} + M_R}{u - M_R^2 + iM_R\Gamma_R}\right)\slashed{p}_\eta\Gamma_s u(p),
$$
$$(49)$$

where $g_{RN\eta}$ is the strong coupling constant, which we have fixed using the $\eta$ production data. The vertex function $\Gamma_{\frac{1}{2}\pm}^\mu$ for the positive and negative parity resonances is given in Eqs. (65) and (66), respectively, where the vector current $V_{\frac{1}{2}}^\mu$ in the case of electroproduction processes is expressed in terms of the $Q^2$ dependent form factors $F_{1,2}^{R^+,R^0}(Q^2)$ as

$$
V_{\frac{1}{2}}^\mu = \frac{F_1^R(Q^2)}{(2M)^2}(\slashed{q}q^\mu + Q^2\gamma^\mu) + \frac{F_2^R(Q^2)}{2M}i\sigma^{\mu\nu}q_\nu, \quad R = R^+, R^0.
$$
$$(50)$$

The electromagnetic transition form factors for the charged $[F_{1,2}^{R^+}(Q^2)]$ and neutral $[F_{1,2}^{R^0}(Q^2)]$ states are then related to the helicity amplitudes given by the following relations [13];

$$
A_{\frac{1}{2}} = \sqrt{\frac{2\pi\alpha}{K_R}}\left\langle R, J_Z = \frac{1}{2}\middle|\epsilon_\mu^+ J_i^\mu\middle|N, J_Z = \frac{-1}{2}\right\rangle\zeta
$$
$$
S_{\frac{1}{2}} = -\sqrt{\frac{2\pi\alpha}{K_R}}\frac{|\vec{q}|}{\sqrt{Q^2}}\left\langle R, J_Z = \frac{1}{2}\middle|\epsilon_\mu^0 J_i^\mu\middle|N, J_Z = \frac{-1}{2}\right\rangle\zeta
$$
$$(51)$$

where in the resonance rest frame,

$$
K_R = \frac{M_R^2 - M^2}{2M_R}, \qquad |\vec{q}|^2 = \frac{(M_R^2 - M^2 - Q^2)^2}{4M_R^2} + Q^2,
$$
$$
\epsilon_\pm^\mu = \mp\frac{1}{\sqrt{2}}(0, 1, \pm i, 0), \qquad \epsilon_0^\mu = \frac{1}{\sqrt{Q^2}}(|\vec{q}|, 1, 0, q^0).
$$
$$(52)$$

The parameter $\zeta$ is model dependent which is related to the sign of $R \to N\pi$, and for the present calculation is taken as $\zeta = 1$.

Using Eq. (52) in Eq. (51), the helicity amplitudes $A_{\frac{1}{2}}(Q^2)$ and $S_{\frac{1}{2}}(Q^2)$ in terms of the electromagnetic form factors $F_1^{R^+,R^0}$ and $F_2^{R^+,R^0}$ are obtained as [55]:

$$
A_{\frac{1}{2}}^{p,n}(Q^2) = \sqrt{\frac{2\pi\alpha}{M}\frac{(M_R + M)^2 + Q^2}{M_R^2 - M^2}}\left(\frac{Q^2}{4M^2}F_1^{R^+,R^0}(Q^2) + \frac{M_R - M}{2M}F_2^{R^+,R^0}(Q^2)\right)
$$
$$
S_{\frac{1}{2}}^{p,n}(Q^2) = \sqrt{\frac{\pi\alpha}{M}\frac{(M_R - M)^2 + Q^2}{M_R^2 - M^2}}\frac{(M_R + M)^2 + Q^2}{4M_RM}\left(\frac{M_R - M}{2M}F_1^{R^+,R^0}(Q^2) - F_2^{R^+,R^0}(Q^2)\right). \quad (53)
$$

The $Q^2$ dependence of the helicity amplitudes [Eq. (53)] is generally parametrized as [54]:

$$
\mathcal{A}_\alpha(Q^2) = \mathcal{A}_\alpha(0)(1 + \alpha Q^2)e^{-\beta Q^2}, \quad (54)
$$

where $\mathcal{A}_\alpha(Q^2)$ are the helicity amplitudes; $A_{\frac{1}{2}}(Q^2)$ and $S_{\frac{1}{2}}(Q^2)$ and parameters $\mathcal{A}_\alpha(0)$ are generally determined by a fit to the photoproduction data of the corresponding resonance. In the present work, the values of $A_{\frac{1}{2}}(0)$ are taken from the PDG [51]. While the parameters $\alpha$ and $\beta$ for each amplitude are obtained from the

electroproduction data available at different $Q^2$ from the CLAS experiment [60–63], and the values of these parameters for the different nucleon resonances parametrized are tabulated in Table II. The $Q^2$ dependence of the helicity amplitudes for $S_{11}(1535)$, $S_{11}(1650)$, and $P_{11}(1710)$ resonances is described by Eq. (54), which are then used in Eq. (53) to obtain the electromagnetic $F_{1,2}^{R^+,R^0}(Q^2)$ form factors.

In Figs. 5 and 6, we have shown the $Q^2$ dependence of $A_{\frac{1}{2}}^{p,n}$ and $S_{\frac{1}{2}}^{p,n}$, respectively, for $S_{11}(1535)$, $S_{11}(1650)$,
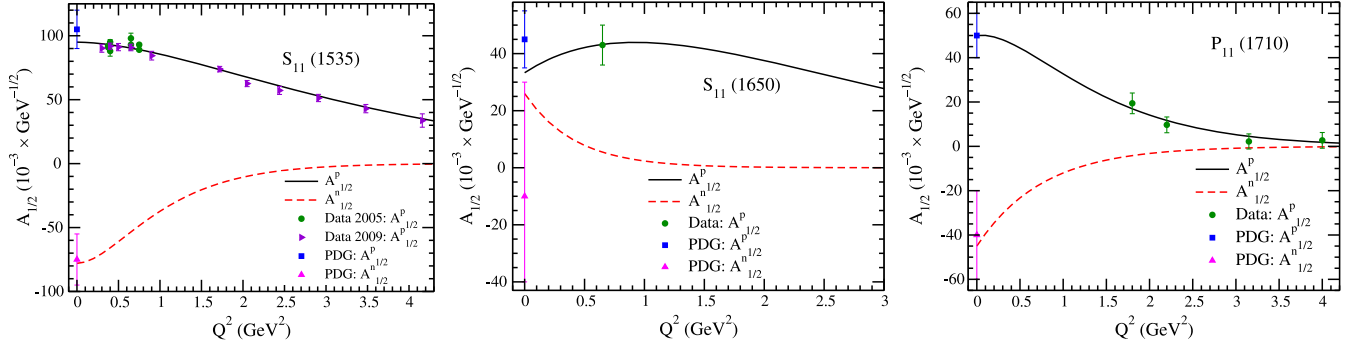
FIG. 5. $Q^2$ dependence of the helicity amplitude $A_{1/2}^{p,n}$ appearing in Eq. (54) for $S_{11}(1535)$ (left panel), $S_{11}(1650)$ (middle panel), and $P_{11}(1710)$ (right panel) resonances. Solid (dashed) lines are our results for $A_{1/2}^p(A_{1/2}^n)$ amplitudes. Solid square (up triangle) are the values of $A_{1/2}^p(A_{1/2}^n)$ at $Q^2 = 0$ from the PDG [51]. Solid circle and right triangle are the data points available from the CLAS experiment [60–63].
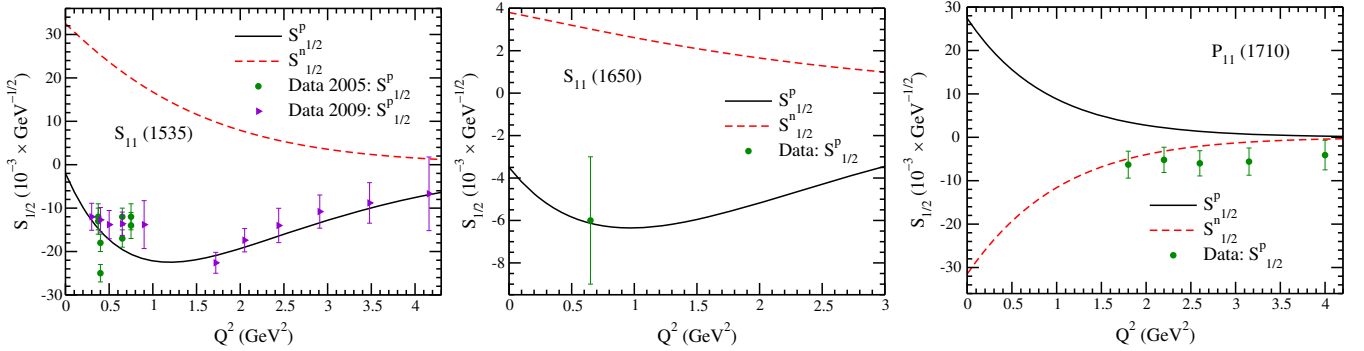


FIG. 6. $Q^2$ dependence of the helicity amplitude $S_{1/2}^{p,n}$ given in Eq. (54) for $S_{11}(1535)$ (left panel), $S_{11}(1650)$ (middle panel), and $P_{11}(1710)$ (right panel) resonances. Lines and points have the same meaning as in Fig. 5.

and $P_{11}(1710)$ resonances. The values of $A_{\frac{1}{2}}^{p,n}(0)$ are taken from PDG [51]. The data points shown in these figures are obtained from the analysis of the experimentally measured differential cross sections, longitudinally polarized beam asymmetries, and longitudinal target and beam-target asymmetries for $\pi$ and $\eta$ electroproductions from the proton target available from the CLAS experiment [60–63]. To determine the helicity amplitudes

at the different values of $Q^2$, in Refs. [60–63] the experimental data are analyzed using the two different approaches viz. dispersion relations and a unitary isobar model, and the final results are the average of the two analyses. The $Q^2$ dependence of the electromagnetic form factors $F_i^{R^+,R^0}(Q^2)$; ($i = 1, 2$) for the resonances $S_{11}(1535)$, $S_{11}(1650)$, and $P_{11}(1710)$ are presented in Fig. 7.
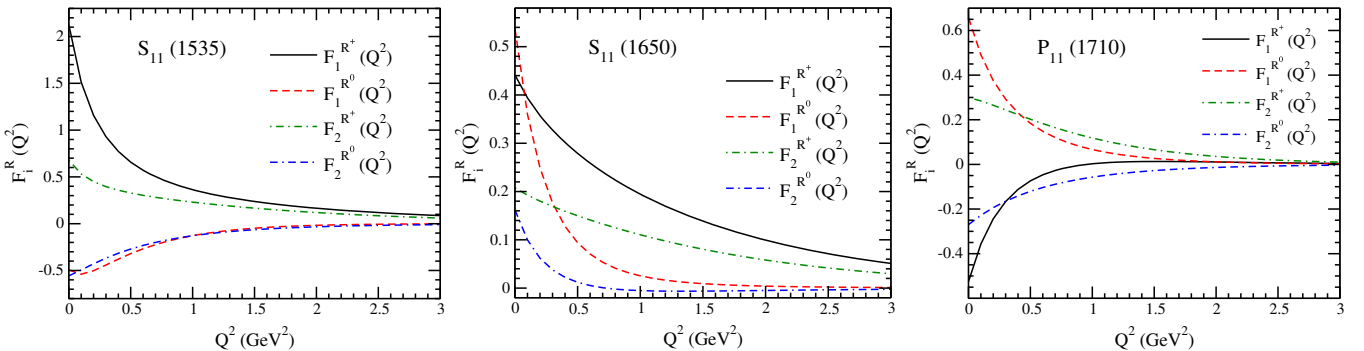


FIG. 7. $Q^2$ dependence of the electromagnetic form factors $F_i^{R^+,R^0}(Q^2)$; ($i = 1, 2$) given in Eq. (53) for $S_{11}(1535)$ (left panel), $S_{11}(1650)$ (middle panel), and $P_{11}(1710)$ (right panel) resonances.
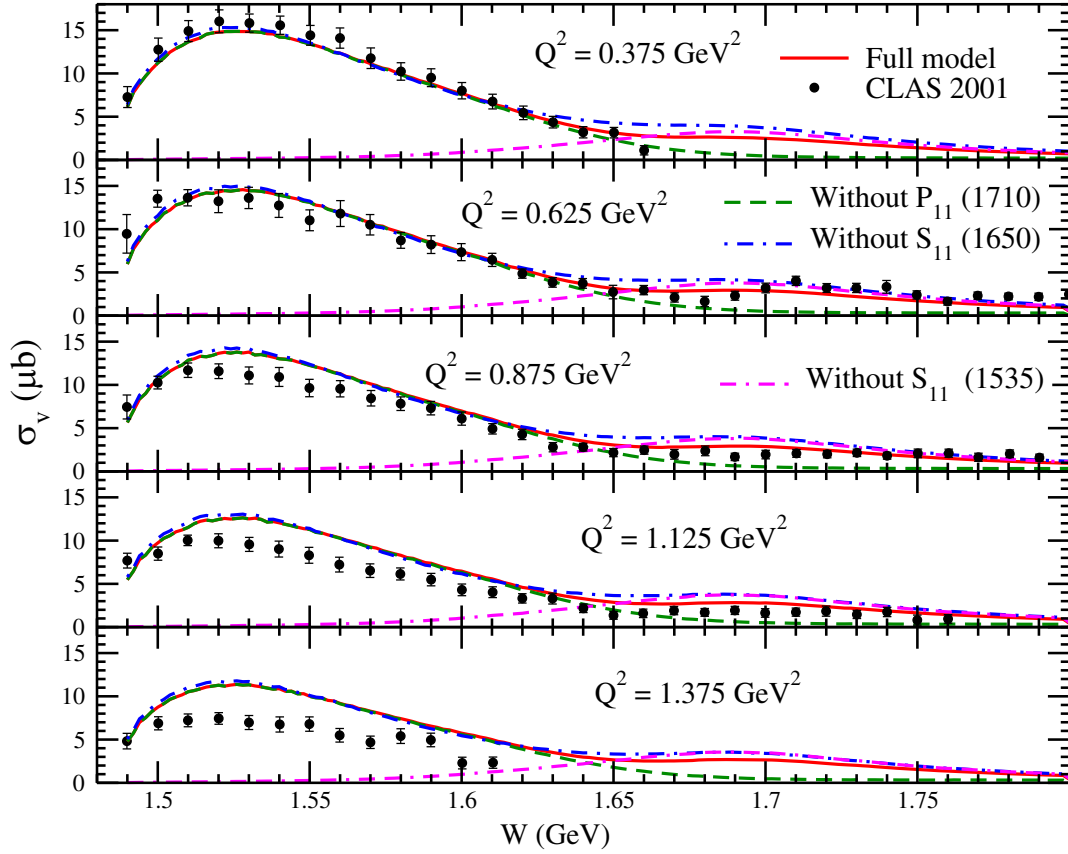
FIG. 8.    Integrated cross section $\sigma_v$ vs $W$ at different $Q^2$ for $\gamma^* p \to \eta p$ process. The experimental points are taken from the CLAS data [16]. Solid line shows the results of the full model which receives contribution from the nonresonant Born terms as well as from the nucleon resonance excitations. Double-dashed-dotted, dashed-dotted, and dashed lines, respectively, show the results of the full model without $S_{11}(1535)$, $S_{11}(1650)$, and $P_{11}(1710)$ resonances.

Using the expressions of the hadronic currents given in Eqs. (46) and (49), respectively, for the nonresonant Born terms and resonance excitations, and the leptonic current given in Eq. (41) in Eq. (43), we obtain the angular distribution $(\frac{d\sigma_v}{d\Omega_{qp_\eta}})$ of the scattering of virtual photons with proton. Performing integration over $\cos\theta_{qp_\eta}$ and $\phi_{qp_\eta}$, we obtain the total cross section $\sigma_v$ for $\gamma^* p \to \eta p$ process, which is presented in Fig. 8 as a function of c.m. energy $W$ at different values of $Q^2$ viz. $Q^2 = 0.375, 0.625, 0.875, 1.125$, and $1.375$ GeV$^2$. The theoretical calculations presented as the full model receives contribution from the nonresonant Born terms as well as from the $S_{11}(1535)$, $S_{11}(1650)$, and $P_{11}(1710)$ resonances. In order to depict the individual contribution of the different nucleon resonances to the total cross section, we have also presented the results for the full model by switching off the contribution of an individual resonance. It may be observed from the figure that at all values of $Q^2$, the first peak region around $W \sim 1.52$ GeV is dominated by $S_{11}(1535)$ resonance while in the region of $W > 1.65$ GeV, the relative contribution from $P_{11}(1710)$ becomes significant. We have also compared our theoretical calculations with the experimental

data available from the CLAS experiment [16] and found a good agreement between the experimental and theoretical results especially in the low $Q^2$ region. An important point to mention here is that the contribution from the nonresonant background terms is quite small in the c.m. energy region considered in the present work. This implies that the $\eta$ electroproduction (Fig. 8) as well as the photoproduction (Fig. 3) is dominated by the resonant production, $S_{11}(1535)$ in the region of $W \leq 1.65$ GeV, beyond which the contribution from the other resonances become important. Indeed, the present work justifies the resonance production model used by various authors in describing the electromagnetic production of $\eta$ mesons [25–28,32,35]. However, the contribution of the nonresonant terms may be important for the other physical observables like beam and/or target polarizations [27].

### C. $\eta$ production induced by (anti)neutrinos

(Anti)neutrino induced single $\eta$ production off the nucleon target (Fig. 2) are given by the following reactions

$$\nu_\mu(k) + n(p) \to \mu^-(k') + \eta(p_\eta) + p(p'), \quad (55)$$

$$\bar{\nu}_\mu(k) + p(p) \rightarrow \mu^+(k') + \eta(p_\eta) + n(p'), \quad (56)$$

where the quantities in the parenthesis are the four momenta of the particles.

Using the general expression of the differential scattering cross section given in Eq. (39) for the reactions shown in Eqs. (55) and (56), the double differential scattering cross section $\frac{d\sigma}{dQ^2 dW}$, in the laboratory frame, is obtained as

$$\frac{d\sigma}{dQ^2 dW} = \int_0^{2\pi} d\phi_{qp_\eta}$$
$$\times \int_{E_\eta^{\min}}^{E_\eta^{\max}} dE_\eta \frac{1}{(2\pi)^4} \frac{1}{64 E_\nu^2 M^2} \frac{W}{|\vec{q}|} \overline{\sum}\sum |\mathcal{M}|^2, \quad (57)$$

where $W = \sqrt{(p+q)^2}$ is the hadronic c.m. energy. The transition matrix element $\mathcal{M}$, in the case of weak interaction induced process, is given by

$$\mathcal{M} = \frac{G_F}{\sqrt{2}} \cos\theta_C l_\mu J^\mu, \quad (58)$$

with $G_F$ being the Fermi coupling constant and $\theta_C$ being the Cabibbo mixing angle. The leptonic current $l_\mu$ is given

$$l_\mu = \bar{u}(k')\gamma_\mu(1-\gamma_5)u(k) \quad (59)$$

and $J^\mu$ is the weak hadronic current, which receives contribution from the vector and axial vector charged currents. We have earlier seen in Sec. II B that the electromagnetic production of $\eta$ is dominated by the resonance production and the contribution of the background terms is small. However, this treatment of the dominant resonance production model has not been applied in the weak production of $\eta$. We, therefore, consider the contribution of the nonresonant ($J_{NR}^\mu$) as well as resonant ($J_R^\mu$) terms and write $J^\mu$ as $J^\mu = J_{NR}^\mu + J_R^\mu$.

The hadronic currents for the Born diagrams (s- and u-channels) with nucleon poles, using the nonlinear sigma model discussed in Sec. II A 1, are given in Eq. (49), except for the fact that $\mathcal{O}_N$ is now replaced by $\mathcal{O}_V$ where $\mathcal{O}_V = V^\mu - A^\mu$ is the weak vertex factor and $V^\mu$ and $A^\mu$ are defined in terms of the weak vector and axial-vector form factors as

$$V^\mu = f_1^V(Q^2)\gamma^\mu + \frac{f_2^V(Q^2)}{2M} i\sigma^{\mu\nu} q_\nu, \quad (60)$$

$$A^\mu = \left[ g_1(Q^2)\gamma^\mu + \frac{g_3(Q^2)}{M} q^\mu \right]\gamma_5, \quad (61)$$

where $f_{1,2}^V(Q^2)$ are respectively the isovector form factors, and $g_1(Q^2)$ and $g_3(Q^2)$ are the axial vector and

pseudoscalar form factors. The two isovector form factors $f_{1,2}^V(Q^2)$ are expressed in terms of the Dirac [$F_1^{p,n}(Q^2)$] and Pauli [$F_2^{p,n}(Q^2)$] form factors, discussed in Sec. II B 1, for the protons and the neutrons using the relationships,

$$f_{1,2}^V(Q^2) = F_{1,2}^p(Q^2) - F_{1,2}^n(Q^2). \quad (62)$$

These electromagnetic form factors may be rewritten in terms of Sachs' form factors using Eq. (48).

The axial form factor, $g_1(Q^2)$ is parametrized as

$$g_1(q^2) = g_A(0) \left[ 1 + \frac{Q^2}{M_A^2} \right]^{-2}, \quad (63)$$

where $g_A(0) = 1.267$ is the axial charge and $M_A$ is the axial dipole mass, which in the numerical calculations is taken as the world average value, i.e., $M_A = 1.026$ GeV [64]. On the other hand pseudoscalar form factor $g_3(Q^2)$ may be expressed in terms of $g_1(Q^2)$ using the PCAC hypothesis and Goldberger-Treiman relation as,

$$g_3(Q^2) = \frac{2M g_1(Q^2)}{m_\pi^2 + Q^2}, \quad (64)$$

with $m_\pi$ as the pion mass.

Next, we discuss the positive and negative parity resonance excitation mechanism for the weak interaction induced $\eta$ production. The general expression of the hadronic current for the $s-$ and $u-$channel resonance excitations and their subsequent decay to $N\eta$ mode are given in Eq. (49), where the vertex factor $\Gamma_{\frac{1}{2}\pm}^\mu$ is now written as

$$\Gamma_{\frac{1}{2}+}^\mu = V_{\frac{1}{2}}^\mu - A_{\frac{1}{2}}^\mu, \quad (65)$$

for the positive parity resonance, and as

$$\Gamma_{\frac{1}{2}-}^\mu = (V_{\frac{1}{2}}^\mu - A_{\frac{1}{2}}^\mu)\gamma_5, \quad (66)$$

for the negative parity resonance. The vector and axial vector vertex factors for the weak interaction processes are given by

$$V_{\frac{1}{2}}^\mu = \frac{f_1^{CC}(Q^2)}{(2M)^2}(Q^2\gamma^\mu + \slashed{q}q^\mu) + \frac{f_2^{CC}(Q^2)}{2M} i\sigma^{\mu\alpha} q_\alpha \quad (67)$$

$$A_{\frac{1}{2}}^\mu = \left[ g_1^{CC}(Q^2)\gamma^\mu + \frac{g_3^{CC}(Q^2)}{M} q^\mu \right]\gamma_5, \quad (68)$$

where $f_i^{CC}(Q^2)$ ($i = 1, 2$) are the isovector transition form factors which in turn are expressed in terms of the charged [$F_i^{R+}(Q^2)$] and neutral [$F_i^{R0}(Q^2)$] electromagnetic transition form factors as:

$$f_i^{CC}(Q^2) = F_i^{R+}(Q^2) - F_i^{R0}(Q^2), \quad i = 1, 2 \quad (69)$$

for isospin $\frac{1}{2}$ resonances. Further, these form factors are related to the helicity amplitudes as discussed in Sec. II B 1.

The axial-vector current consists of two form factors viz. $g_1^{CC}(Q^2)$ and $g_3^{CC}(Q^2)$, which are determined assuming the PCAC hypothesis and pion pole dominance of the divergence of the axial-vector current through the generalized GT relation for $N - R$ transition [13]. The divergence of the axial vector current, defined in Eq. (68), is obtained as

$$\partial_\mu A_{\frac{1}{2}}^\mu = \bar{u}(p_R)\left[g_1^{CC}(Q^2)(M_R \pm M) + \frac{g_3^{CC}}{M}q^2\right]\gamma_5\Gamma u(p) \tag{70}$$

where $p_R$ is the four momentum of the resonance, $\Gamma = 1(\gamma_5)$ and $+(-)$ in $M_R \pm M$ stands for the positive (negative) parity resonances.

The Lagrangian at the strong $NR\pi$ vertex is written as

$$\mathcal{L}_{RN\pi} = \sqrt{2}\frac{g_{RN\pi}}{f_\pi}\bar{\Psi}_R\Gamma_s^\mu\partial_\mu\phi_i\tau^i\Psi \tag{71}$$

where $g_{RN\pi}$ is the coupling constant at the strong vertex, $f_\pi$ is the pion decay constant, $\phi$ represents the triplet of the pion field. The value of the strong coupling $g_{RN\pi}$ is obtained using the partial decay width of the resonance to the $N\pi$ mode, using Eq. (34) with $\mathcal{C} = 3$ and $M_\eta$ is replaced by $m_\pi$.

The axial vector current obtained in the pion pole dominance of the divergence of the axial vector current [using Eq. (71)] is given by

$$A_{PP}^\mu = \sqrt{2}\bar{u}(p_R)\frac{g_{RN\pi}}{f_\pi}(M_R \pm M)\gamma_5\Gamma u(p)\frac{\sqrt{2}f_\pi q^\mu}{q^2 - m_\pi^2}. \tag{72}$$

The divergence of the above expression, in the limit of $m_\pi \to 0$, is obtained as

$$\partial_\mu A_{PP}^\mu = 2g_{RN\pi}\bar{u}(p_R)(M_R \pm M)\gamma_5\Gamma u(p). \tag{73}$$

Comparing the term associated with $g_1^{CC}(Q^2)$ at $Q^2 = 0$ in Eq. (70) with the above expression, we obtain

$$g_1^{CC}(0) = 2g_{RN\pi}, \tag{74}$$

with $g_{RN\pi}$ being the coupling strength for $R_{\frac{1}{2}} \to N\pi$ decay, which has been determined by the partial decay width of the resonance and tabulated in Table I. Since no information about the $Q^2$ dependence of the axial-vector form factor is known experimentally, therefore, a dipole form is assumed as in the case of $N \to N'$ or $N \to Y$ transitions:

$$g_1^{CC}(Q^2) = \frac{g_1^{CC}(0)}{\left(1 + \frac{Q^2}{M_A^2}\right)^2}, \tag{75}$$

with $M_A = 1.026$ GeV, and the pseudoscalar form factor $g_3^{CC}(Q^2)$ is given by

$$g_3^{CC}(Q^2) = \frac{(MM_R \pm M^2)}{m_\pi^2 + Q^2}g_1^{CC}(Q^2), \tag{76}$$

where $+(-)$ sign is for positive (negative) parity resonances. However, the contribution of $g_3^{CC}(Q^2)$ being directly proportional to the lepton mass squared is almost negligible.

## III. RESULTS AND DISCUSSION

In Fig. 9, we have presented the results for the $Q^2$ distribution in the charged current $\nu_\mu(\bar{\nu}_\mu)$ induced $\eta$ production from the free nucleon target at $E_{\nu_\mu(\bar{\nu}_\mu)} = 1$ and 1.5 GeV. It may be observed from the figure that at $E_\nu = 1.5$ GeV the results obtained with only $S_{11}(1535)$
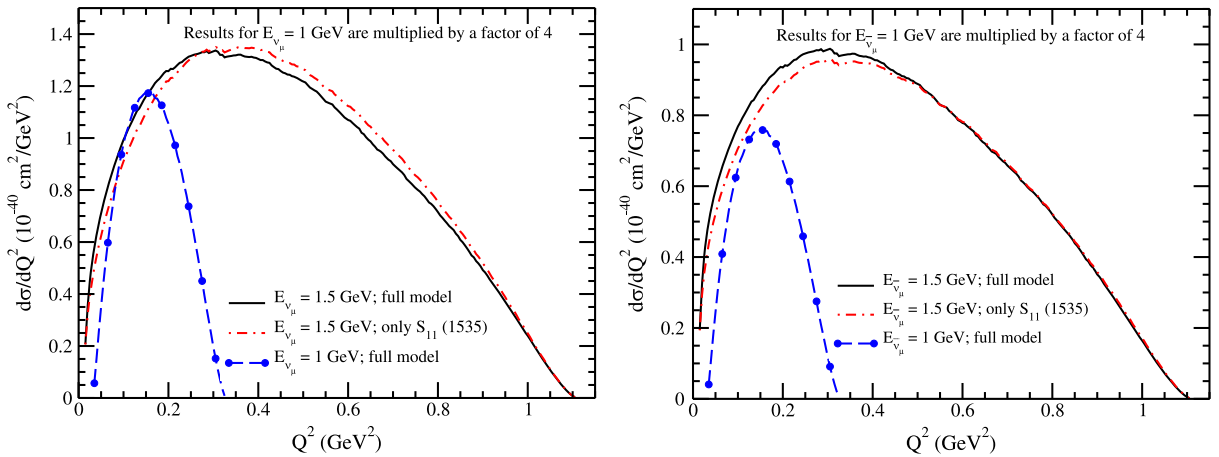


FIG. 9. $Q^2$ distribution for the charged current induced $\nu_\mu + n \to \mu^- + p + \eta$ (left panel) and $\bar{\nu}_\mu + p \to \mu^+ + n + \eta$ (right panel) processes at $E_{\nu_\mu(\bar{\nu}_\mu)} = 1$ GeV (dashed line with circle) and 1.5 GeV (solid line) using the full model calculation. Dashed-dotted line shows the results obtained from $S_{11}(1535)$ resonance only at $E_{\nu_\mu(\bar{\nu}_\mu)} = 1.5$ GeV.
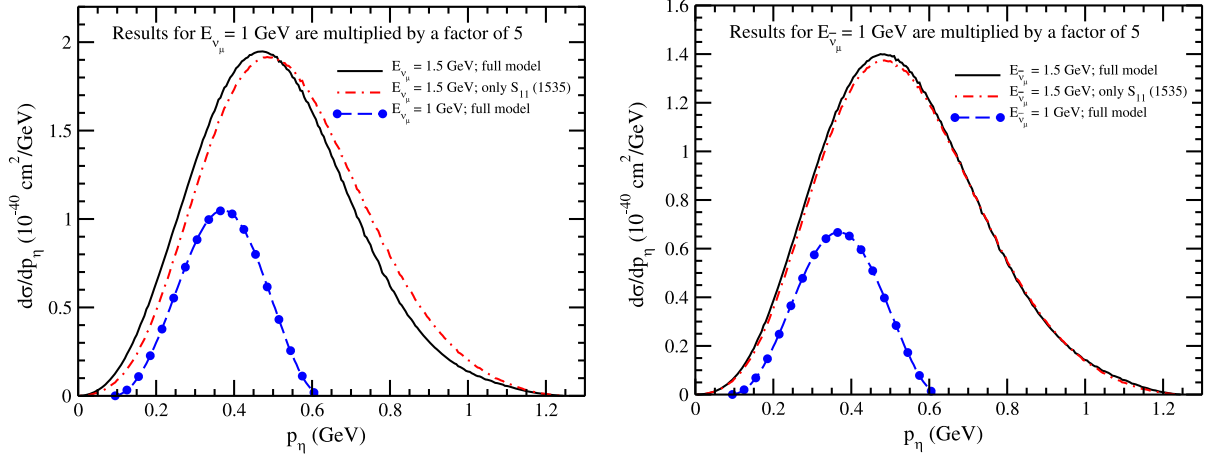
FIG. 10. $\eta$-momentum distribution for the charged current induced $\nu_\mu + n \to \mu^- + p + \eta$ (left panel) and $\bar{\nu}_\mu + p \to \mu^+ + n + \eta$ (right panel) processes. Lines and points have the same meaning as in Fig. 9.

resonance are comparable to the results of the full model in the region of high $Q^2$ region. Even in the low $Q^2$ region, the contribution from the Born terms and other resonances is not more than 10% of the total result. At $E_{\nu_\mu(\bar{\nu}_\mu)} = 1$ GeV, we find that (not shown here) the contribution of the higher resonances and Born terms is almost negligible as compared to the contribution of $S_{11}(1535)$ resonance.

In Fig. 10, we have presented the results for the $\eta$-momentum distribution of $\nu_\mu(\bar{\nu}_\mu)$ induced $\eta$ production from the free nucleon target at $E_{\nu_\mu(\bar{\nu}_\mu)} = 1$ and 1.5 GeV. As in the case of $Q^2$ distribution, we find very small contribution of the Born terms and higher resonances to the $p_\eta$ distribution as compared to the contribution of $S_{11}(1535)$ resonance.

Figure 11 shows the results for the total scattering cross sections for the processes $\nu_\mu + n \to \mu^- + \eta + p$ and $\bar{\nu}_\mu + p \to \mu^+ + \eta + n$. The individual contribution from $S_{11}(1535)$, $S_{11}(1650)$, and $P_{11}(1710)$ resonance excitations, where both the direct and crossed diagrams are considered, the contribution from the background terms, as well as the full model (sum of all the diagrams) are shown. It may be observed from the figure that in the case of both neutrino and antineutrino induced reactions, $S_{11}(1535)$ has the dominant contribution followed by $P_{11}(1710)$ and $S_{11}(1650)$ resonances. In the case of neutrino induced $\eta$ production process, the background terms are almost an order of magnitude smaller than the results of the full model. While in the case of antineutrino channel, the
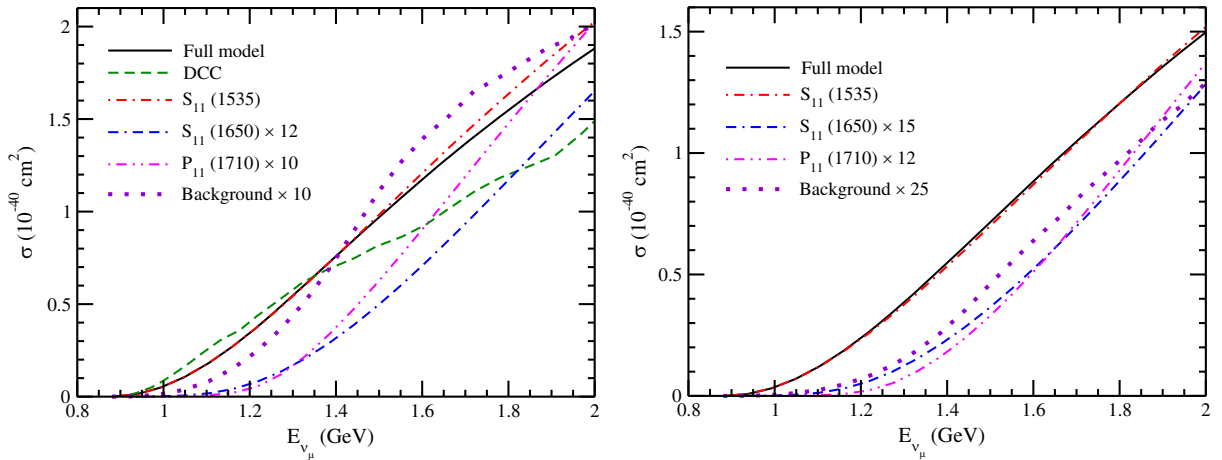


FIG. 11. Total scattering cross section for CC induced $\eta$ production, i.e., $\nu_\mu + n \to \mu^- + \eta + p$ (left panel) and $\bar{\nu}_\mu + p \to \mu^+ + \eta + n$ (right panel). Full model (solid line) consists of the contributions from all the diagrams including $S_{11}(1535)$, $S_{11}(1650)$, and $P_{11}(1710)$. The individual contribution from $S_{11}(1535)$, $S_{11}(1650)$, and $P_{11}(1710)$ resonances are shown by dashed-dotted, double-dashed-dotted, and double-dotted-dashed lines, respectively, and the contribution from the nonresonant background terms are shown by dotted line. In the case of neutrino induced $\eta$ production, we have also compared our results of the full model with the results obtained in the DCC model by Nakamura *et al.* [3]. Notice the different multiplicative factors used in the results of background terms as well as $S_{11}(1650)$ and $P_{11}(1710)$ resonances to bring them on the same scale as that of the results obtained using the full model.
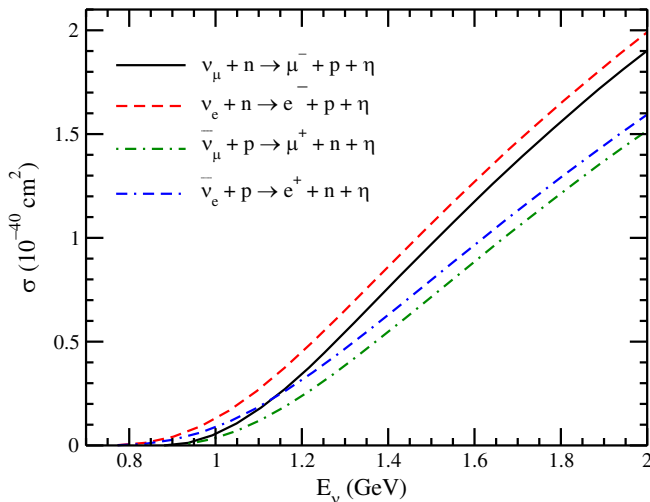
FIG. 12. Total scattering cross section for CC induced $\eta$ production, i.e., $\nu_\mu + n \rightarrow \mu^- + \eta + p$ (solid line), $\nu_e + n \rightarrow e^- + \eta + p$ (dashed line), $\bar{\nu}_\mu + p \rightarrow \mu^+ + \eta + n$ (dashed-dotted line), and $\bar{\nu}_e + p \rightarrow e^+ + \eta + n$ (double-dashed-dotted line).

contribution of the background terms is even further smaller. We have also compared the present results for the neutrino induced $\eta$ production with the results of DCC model [3] and found that from threshold up to $E_{\nu_\mu} \sim$ 1.3 GeV our results are consistent with the results of DCC model. While for $E_{\nu_\mu} > 1.3$ GeV, our results are higher than the results obtained using DCC model.

To explicitly show the lepton mass effect, in Fig. 12, we have presented the results for the total scattering cross section for the $\eta$ production induced by $\nu_e(\bar{\nu}_e)$ and $\nu_\mu(\bar{\nu}_\mu)$. It may be noticed that due to the lower threshold for $\nu_e(\bar{\nu}_e)$, the cross section is larger than that of $\nu_\mu(\bar{\nu}_\mu)$ induced processes even at $E_{\nu(\bar{\nu})} = 2$ GeV. Since the value of axial dipole mass is in debate as the different neutrino experiment quote different values of $M_A$ ranging from 1 to 1.3 GeV, therefore, in the case of $\eta$ production, we have studied the effect of $M_A$ on the total scattering cross section (not shown here) by varying it in the range $\pm 10\%$ for the Born as well as the resonance terms. We find that the effect of $M_A$ variation is less than 5%, even at $E_{\nu_\mu(\bar{\nu}_\mu)} = 2$ GeV.

## IV. SUMMARY AND CONCLUSIONS

In summary, we have studied the charged current $\nu_\mu(\bar{\nu}_\mu)$ induced $\eta$ production off the nucleons and presented the results for the total scattering cross section $\sigma(E_{\nu_\mu(\bar{\nu}_\mu)})$, $Q^2$-distribution $\left(\frac{d\sigma}{dQ^2}\right)$ and the momentum distribution $\left(\frac{d\sigma}{dp_\eta}\right)$ for the $\eta$ mesons, in a model in which the contribution from the nonresonant Born terms and the resonant terms are calculated in an effective Lagrangian approach. The parameters

of the model for evaluating the vector current contribution have been fixed by fitting the experimental data on the total cross sections of the photo- and electro-production on the nucleons from the MAINZ and CLAS experiments. The vector part of the $N \rightarrow R$ transition form factors has been obtained from the MAID helicity amplitudes while the axial vector part is obtained with the help of PCAC hypothesis and assuming the pion-pole dominance of the divergence of the axial vector current. For the nonresonant background terms we have used a microscopical model based on the SU(3) chiral Lagrangians. The parameters of the model are meson decay constants, Cabibbo's angle, the proton and neutron magnetic moments, all of which are known with good accuracy, and the parameters $D$ and $F$ obtained from the analysis of the hyperon semileptonic decays.

The results are summarized as

(i) In the electromagnetic sector, the cross section is dominated by the contribution from $S_{11}(1535)$ resonance, especially at low $W$. With the increase in $W$ the contribution from $P_{11}(1710)$ starts to show up and around $W \geq 1.7$ GeV its contribution is larger than the other resonances.

(ii) In the weak sector, $S_{11}(1535)$ resonance dominates even at $E_\nu = 2$ GeV, while the contribution of $S_{11}(1650)$ is not more than 7% of the total scattering cross section, while that of $P_{11}(1710)$ is about 10%.

(iii) The $Q^2$ distribution has a peak at $Q^2 \approx$ 0.15(0.28) GeV$^2$ at $E_{\nu_\mu} = 1(1.5)$ GeV. The nature of $Q^2$ distribution in the antineutrino channel is almost similar to that observed in the neutrino case.

(iv) The eta momentum distribution has a peak at $p_\eta \approx 0.37(0.47)$ GeV at $E_{\nu_\mu} = 1(1.5)$ GeV. The nature of momentum distribution in the antineutrino channel is almost similar to that observed in the neutrino case.

To conclude, the results obtained in this work may be very useful in studying the feasibility of observing the weak production of $\eta$ in experiments like MicroBooNE, T2K, NOvA, MINERvA and the next generation experiments like T2-HyperK and DUNE. Furthermore, the study of $\eta$ production is also important in the analysis of atmospheric neutrino events.

[1] M. Sajjad Athar, S. W. Barwick, T. Brunner, J. Cao, M. Danilov, K. Inoue, T. Kajita, M. Kowalski, M. Lindner, K. R. Long *et al.*, Prog. Part. Nucl. Phys. **124**, 103947 (2022).

[2] N. Dombey, Phys. Rev. **174**, 2127 (1968).

[3] S. X. Nakamura, H. Kamano, and T. Sato, Phys. Rev. D **92**, 074024 (2015).

[4] C. Thorpe (MicroBooNE Collaboration), https://indico .cern.ch/event/881216/contributions/5048785/attachments/ 2536274/4365114/nuint_2022_talk.pdf.

[5] C. B. Dover and P. M. Fishbane, Phys. Rev. Lett. **64**, 3115 (1990).

[6] D. Drechsel, S. S. Kamalov, and L. Tiator, Eur. Phys. J. A **34**, 69 (2007).

[7] A. Fatima, Z. Ahmad Dar, M. Sajjad Athar, and S. K. Singh, Int. J. Mod. Phys. E **29**, 2050051 (2020).

[8] M. Rafi Alam, M. Sajjad Athar, S. Chauhan, and S. K. Singh, Int. J. Mod. Phys. E **25**, 1650010 (2016).

[9] M. Rafi Alam, M. Sajjad Athar, L. Alvarez-Ruso, I. Ruiz Simo, M. J. Vicente Vacas, and S. K. Singh, arXiv:1311 .2293.

[10] M. Rafi Alam, I. Ruiz Simo, M. Sajjad Athar, and M. J. Vicente Vacas, Phys. Rev. D **82**, 033001 (2010).

[11] M. Rafi Alam, I. Ruiz Simo, M. Sajjad Athar, and M. J. Vicente Vacas, Phys. Rev. D **87**, 053008 (2013).

[12] E. Hernandez, J. Nieves, S. K. Singh, M. Valverde, and M. J. Vicente Vacas, Phys. Rev. D **77**, 053009 (2008).

[13] M. Sajjad Athar, A. Fatima, and S. K. Singh, Prog. Part. Nucl. Phys. **129**, 104019 (2023).

[14] O. Bartholomy *et al.* (CB-ELSA Collaboration), Eur. Phys. J. A **33**, 133 (2007).

[15] V. Crede *et al.* (CBELSA/TAPS Collaboration), Phys. Rev. C **80**, 055202 (2009).

[16] R. Thompson *et al.* (CLAS Collaboration), Phys. Rev. Lett. **86**, 1702 (2001).

[17] H. Denizli *et al.* (CLAS Collaboration), Phys. Rev. C **76**, 015204 (2007).

[18] E. F. McNicoll *et al.* (Crystal Ball at MAMI Collaboration), Phys. Rev. C **82**, 035208 (2010); **84**, 029901(E) (2011).

[19] D. Werthmüller *et al.* (A2 Collaboration), Phys. Rev. C **90**, 015205 (2014).

[20] C. S. Armstrong *et al.* (Jefferson Lab E94014 Collaboration), Phys. Rev. D **60**, 052004 (1999).

[21] F. Renard *et al.* (GRAAL Collaboration), Phys. Lett. B **528**, 215 (2002).

[22] L. Witthauer *et al.* (A2 Collaboration), Phys. Rev. C **95**, 055201 (2017).

[23] J. W. Price, G. Anton, J. Arends, W. Beulertz, A. Bock, M. Breuer, K. Buechler, M. Clajus, P. Detemple, J. Hey *et al.*, Phys. Rev. C **51**, R2283 (1995).

[24] B. Krusche, J. Ahrens, G. Anton, R. Beck, M. Fuchs, A. R. Gabler, F. Harter, S. Hall, P. Harty, S. Hlavac *et al.*, Phys. Rev. Lett. **74**, 3736 (1995).

[25] J. Lehr and U. Mosel, Phys. Rev. C **68**, 044603 (2003).

[26] J. Lehr, M. Post, and U. Mosel, Phys. Rev. C **68**, 044601 (2003).

[27] G. Knochlein, D. Drechsel, and L. Tiator, Z. Phys. A **352**, 327 (1995).

[28] B. Krusche and C. Wilkin, Prog. Part. Nucl. Phys. **80**, 43 (2015).

[29] A. Fix and H. Arenhovel, Eur. Phys. J. A **19**, 275 (2004).

[30] D. Ruić, M. Mai, and U. G. Meissner, Phys. Lett. B **704**, 659 (2011).

[31] M. Benmerrouche and N. C. Mukhopadhyay, Phys. Rev. Lett. **67**, 1070 (1991).

[32] M. Benmerrouche, N. C. Mukhopadhyay, and J. F. Zhang, Phys. Rev. D **51**, 3237 (1995).

[33] L. Tiator, C. Bennhold, and S. S. Kamalov, Nucl. Phys. **A580**, 455 (1994).

[34] C. Deutsch-Sauermann, B. Friman, and W. Norenberg, Phys. Lett. B **409**, 51 (1997).

[35] W. T. Chiang, S. N. Yang, L. Tiator, and D. Drechsel, Nucl. Phys. **A700**, 429 (2002).

[36] T. Feuster and U. Mosel, Phys. Rev. C **59**, 460 (1999).

[37] R. M. Davidson, N. Mathur, and N. C. Mukhopadhyay, Phys. Rev. C **62**, 058201 (2000).

[38] M. Kirchbach and L. Tiator, Nucl. Phys. **A604**, 385 (1996).

[39] S. Neumeier and M. Kirchbach, Int. J. Mod. Phys. A **15**, 4325 (2000).

[40] H. Kamano, T. S. H. Lee, S. X. Nakamura, and T. Sato, arXiv:1909.11935.

[41] E. Breitmoser and H. Arenhovel, Nucl. Phys. **A612**, 321 (1997).

[42] V. Kuznetsov *et al.*, Acta Phys. Pol. B **39**, 1949 (2008).

[43] A. S. Rosenthal, T. Forest, and M. Gonzales, Phys. Rev. C **44**, 2765 (1991).

[44] R. Bradford *et al.* (CLAS Collaboration), Phys. Rev. C **73**, 035202 (2006).

[45] E. Hernandez, J. Nieves, and M. Valverde, Phys. Rev. D **76**, 033005 (2007).

[46] O. Lalakulich, T. Leitner, O. Buss, and U. Mosel, Phys. Rev. D **82**, 093001 (2010).

[47] T. Sato, D. Uno, and T. S. H. Lee, Phys. Rev. C **67**, 065201 (2003).

[48] S. Scherer, Adv. Nucl. Phys. **27**, 277 (2003).

[49] S. Scherer and M. R. Schindler, Lect. Notes Phys. **830**, 1 (2012).

[50] A. Faessler, T. Gutsche, B. R. Holstein, M. A. Ivanov, J. G. Korner, and V. E. Lyubovitskij, Phys. Rev. D **78**, 094005 (2008).

[51] P. A. Zyla *et al.* (Particle Data Group), Prog. Theor. Exp. Phys. **2020**, 083C01 (2020).

[52] D. Skoupil and P. Bydžovský, Phys. Rev. C **93**, 025204 (2016).

[53] M. S. Athar and S. K. Singh, *The Physics of Neutrino Interactions* (Cambridge University Press, Cambridge, England, 2020), ISBN 978-1-108-77383-6, 978-1-108-48906-5.

[54] L. Tiator, D. Drechsel, S. S. Kamalov, and M. Vanderhaeghen, Eur. Phys. J. Special Topics **198**, 141 (2011).

[55] T. Leitner, O. Buss, L. Alvarez-Ruso, and U. Mosel, Phys. Rev. C **79**, 034601 (2009).

[56] A. Donnachie and G. Shaw, *Electromagnetic Interactions of Hadrons* (Springer, New York, 1978), 446p.

[57] E. Amaldi, S. Fubini, and G. Furlan, Springer Tracts Mod. Phys. **83**, 1 (1979).

[58] D. Drechsel, Few Body Syst. Suppl. **7**, 325 (1994).

[59] R. Bradford, A. Bodek, H. S. Budd, and J. Arrington, Nucl. Phys. B, Proc. Suppl. **159**, 127 (2006).

[60] I. G. Aznauryan, V. D. Burkert, H. Egiyan, K. Joo, R. Minehart, and L. C. Smith, Phys. Rev. C **71**, 015201 (2005).

[61] I. G. Aznauryan, V. D. Burkert, G. V. Fedotov, B. S. Ishkhanov, and V. I. Mokeev, Phys. Rev. C **72**, 045201 (2005).

[62] I. G. Aznauryan *et al.* (CLAS Collaboration), Phys. Rev. C **80**, 055203 (2009).

[63] K. Park *et al.* (CLAS Collaboration), Phys. Rev. C **91**, 045203 (2015).

[64] V. Bernard, L. Elouadrhiri, and U. G. Meissner, J. Phys. G **28**, R1 (2002).